Dalton Transactions

ROYAL SOCIETY OF CHEMISTRY

PAPER

View Article Online
View Journal | View Issue

Cite this: *Dalton Trans.*, 2024, **53**, 10947

Exploring the potential of ruthenium(II)–phosphine–mercapto complexes as new anticancer agents†

Marcos V. Palmeira-Mello, [a,b] Analu R. Costa, [a] Leticia P. de Oliveira,[a] Olivier Blacque, [c] Gilles Gasser *[b] and Alzir A. Batista *[a]

The search for new metal-based anticancer drug candidates is a fundamental task in medicinal inorganic chemistry. In this work, we assessed the potential of two new Ru(II)–phosphine–mercapto complexes as potential anticancer agents. The complexes, with the formula [Ru(bipy)(dppen)(Lx)]PF_6 [(**1**), **HL1** = 2-mercapto–pyridine and (**2**), **HL2** = 2-mercapto–pyrimidine, bipy = 2,2′-bipyridine, dppen = *cis*-1,2-bis(diphenylphosphino)-ethylene] were synthesized and characterized by nuclear magnetic resonance (NMR) [^{1}H, ^{31}P(^{1}H), and ^{13}C], high resolution mass spectrometry (HR-MS), cyclic voltammetry, infrared and UV-Vis spectroscopies. Complex **2** was obtained as a mixture of two isomers, **2a** and **2b**, respectively. The composition of these metal complexes was confirmed by elemental analysis and liquid chromatography-mass spectrometry (LC-MS). To obtain insights into their lipophilicity, their distribution coefficients between *n*-octanol/PBS were determined. Both complexes showed affinity mainly for the organic phase, presenting positive log *P* values. Also, their stability was confirmed over 48 h in different media (*i.e.*, DMSO, PBS and cell culture medium) *via* HPLC, UV-Vis and ^{31}P{^{1}H} NMR spectroscopies. Since enzymes from the P-450 system play a crucial role in cellular detoxification and metabolism, the microsomal stability of **1**, which was found to be the most interesting compound of this study, was investigated using human microsomes to verify its potential oxidation in the liver. The analyses by LC-MS and ESI-MS reveal three main metabolites, obtained by oxidation in the dppen and bipy moieties. Moreover, **1** was able to interact with human serum albumin (HSA). The cytotoxicity of the metal complexes was tested in different cancerous and non-cancerous cell lines. Complex **1** was found to be more selective than cisplatin against MDA-MB-231 breast cancer cells when compared to MCF-10A non-cancerous cells. In addition, complex **1** affects cell morphology and migration, and inhibits colony formation in MDA-MB-231 cells, making it a promising cytotoxic agent against breast cancer.

Received 22nd April 2024,
Accepted 1st June 2024

DOI: 10.1039/d4dt01191k

rsc.li/dalton

Introduction

Cancer is a genetic disease associated with uncontrollable cell growth that can infiltrate normal tissues and spread throughout the body. Cancer cells present a microenvironment with different characteristics compared to normal cells such as dysregulated metabolism, resisting cell death, non-functional angiogenesis, high ATP demand, and low oxygen supply.[1,2] Almost 19.3 million cases of cancer were reported in 2020. Breast cancer was the most commonly diagnosed cancer with almost 2.3 million cases.[3] The treatment depends on several factors such as the subtype and the stage. A combination of chemotherapy, radiotherapy, and surgery (when it is possible) is so far the best strategy to avoid recurrence.[4]

Platinum-based compounds have been employed in anticancer chemotherapy.[5–7] Usually their mechanism of action involves the formation of platinum-DNA adducts which arise from covalent bonds between the platinum center and purine-N7 position of guanine or adenine residues.[8] Although their efficacy has been demonstrated, several problems related to platinum drugs resistance are reported, which arise from enhanced efflux and consequently, the reduced accumulation of platinum drugs.[9] In addition to platinum, several metals have been investigated as potential anticancer agents.[10–19]

For example, ruthenium-based compounds are considered promising alternatives to platinum complexes, exhibiting

[a]*Departament of Chemistry, Universidade Federal de São Carlos, 13561-901, São Carlos, SP, Brazil. E-mail: daab@ufscar.br*
[b]*Chimie ParisTech, PSL University, CNRS, Institute of Chemistry for Life and Health Sciences, Paris, France. E-mail: gilles.gasser@chimeparistech.psl.eu; https://www.gassergroup.com*
[c]*Department of Chemistry, University of Zurich, Winterthurerstrasse 190, 8057 Zurich, Switzerland*

†Electronic supplementary information (ESI) available. CCDC 2341519. For ESI and crystallographic data in CIF or other electronic format see DOI: https://doi.org/10.1039/d4dt01191k

different chemical and structural characteristics from those presented by platinum drugs.[20–23] Ruthenium complexes in general present an octahedral geometry, which allows variations of ligands in the coordination sphere, and are less susceptible to deactivation by detoxification agents in the biological environment.[24] Several ruthenium(II)-based compounds have reached clinical trials, such as NAMI-A, KP-1019 and BOLD-100 (Fig. 1).[25–27]

The coordination of bioactive ligands to a ruthenium center is one of several strategies that allow the development of new anticancer agents.[28–31] Ruthenium(II)–phosphine complexes, which were primarily known for their catalytic applications, have gained special attention due to their promising cytotoxicity properties.[32–39] In general, the presence of phosphine in the complexes improves their lipophilicity, which is a crucial factor for the stability of the complexes and their internalization and anticancer property.[40,41] In this direction, complexes **1** and **2a**/**2b** (see Scheme 1) were synthesized and characterized. As pharmacokinetics (PK) is an important parameter that can hamper the correlation between *in vitro*/*in vivo* performance,[42–44] we have decided to investigate the formation of potential metabolites from our ruthenium(II)–phosphine complexes. Since CYP P-450 enzymes play an important role in drug metabolism, human liver microsomes (HLM) were used to obtain important insights about the microsomal stability of complex **1** and its possible oxidation in the liver. To the best of our knowledge, this is the first metabolic study involving a Ru(II)–phosphine–mercapto complex. The cytotoxicity of these metal complexes was investigated in MDA-MB-231 (triple negative breast cancer), MCF-7 (breast cancer), and MCF-10A (non-tumor breast epithelial) cell lines. Cell morphology, migration and clonogenic experiments were also performed. We demonstrated that **1** presents anti-migratory capacity and inhibits the colony formation in breast cancer cells, making it a promising anticancer compound.

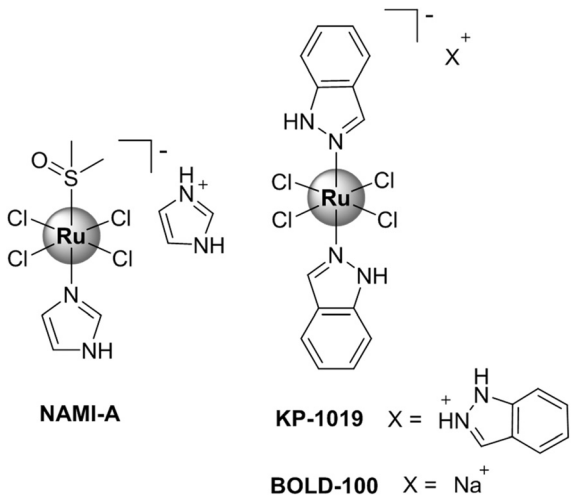

Fig. 1 Chemical structures of ruthenium complexes (NAMI-A, KP-1019 and BOLD-100) that reached clinical trials.

Results and discussion

Metal complexes **1** and **2a**/**2b** were synthesized by refluxing the precursor *cis*-[$RuCl_2$(bipy)(dppen)] (bipy = 2,2′-bipyridine, dppen = *cis*-1,2-bis(diphenylphosphino)-ethylene) with the respective mercapto ligand, 2-mercapto–pyridine (**HL1**) or

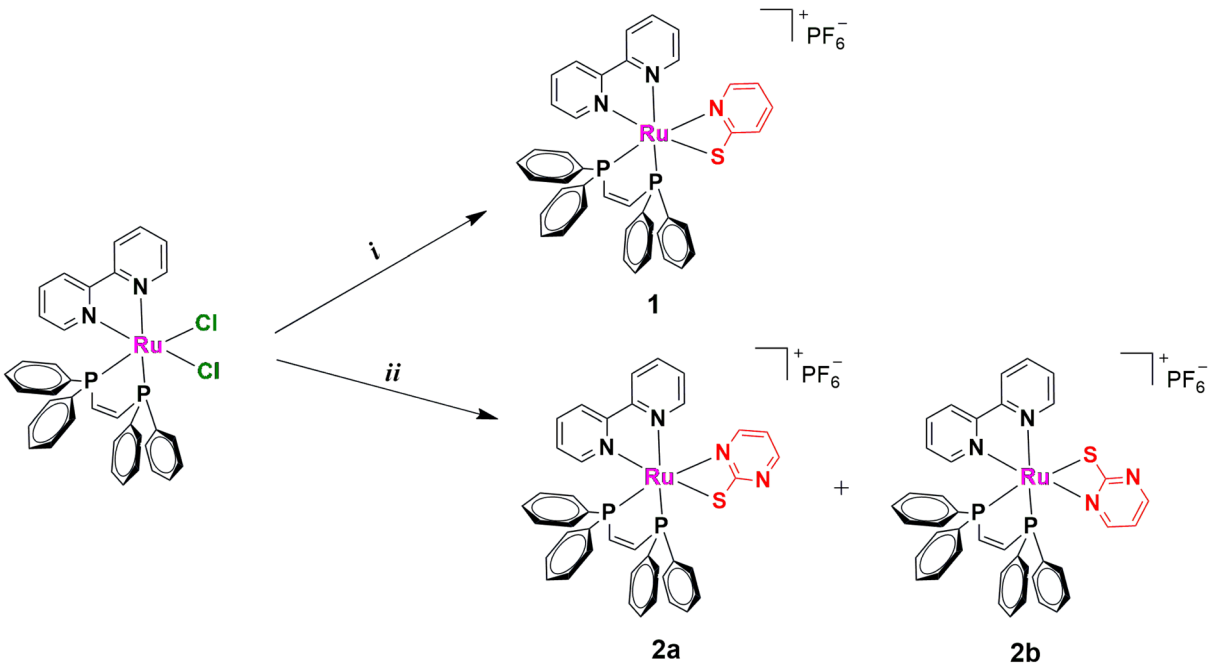

Scheme 1 Synthetic procedures for complexes **1** and **2a**/**2b** (i) 2-mercaptopyridine or 2-mercaptopyrimidine, Et_3N, KPF_6, MeOH/DCM (1 : 1), reflux, 24 h.

2-mercapto–pyrimidine (**HL2**), in MeOH/DCM (1 : 1) in the presence of triethylamine (Scheme 1). Yellow powders were obtained after adding KPF_6 to the reaction mixture. The metal complexes were characterized by NMR [^{1}H, ^{31}P{^{1}H}, and ^{13}C] spectroscopy (Fig. S1–S8†). The ^{31}P{^{1}H} signals in compounds **1** and **2a**/**2b** spectra are shifted to higher frequencies (more deshielding effect) when compared with the precursor *cis*-[$RuCl_2$(bipy)(dppen)] as a consequence of the exchange of chlorido ligands (π- and σ-donor) by the mercapto skeleton (π-acceptor) (Fig. S9†). For **1**, in its ^{31}P{^{1}H}, there is only one set of peaks, two doublets at 77.08 and 74.16 ppm, which are assigned to the two phosphorus atoms (d, J = 11.4 Hz) in the dppen ligand. On the other hand, these signals are duplicated in **2a**/**2b**, and four doublets can be observed at 77.39 and 74.97 ppm (d, J = 11.6 Hz) and at 79.70 and 67.62 ppm (d, J = 6.1 Hz). A similar pattern is observed in the ^{1}H NMR spectrum, indicating the presence of two isomers in solution, **2a** and **2b**, respectively. The first one contains the two phosphorus atoms *trans* to N from bipy and mercapto moieties, and a second one presents one P *trans* to $S_{mercapto}$ and another one coordinated *trans* to N_{bipy}. This behavior was already observed for other Ru(II)–phosphine complexes.[45,46] For **1**, in its ^{31}P{^{1}H} NMR spectrum, there are also signals of two isomers, but in this case, the amount of one of them is insignificant. As expected, in the ^{1}H NMR spectra of **1** and **2a**/**2b**, a heptet around −144 ppm is observed and ascribed to the PF_6^- anion. These findings were confirmed by LC-MS experiments. Results obtained in methanol revealed the presence of only one species for **1** with a retention time (R_T) of 12.47 min (m/z^+ = 764.10). As expected, for **2a**/**2b**, two different peaks can be observed in the chromatogram at 11.55 and 11.19 min, assigned to **2a** and **2b** (m/z^+ = 765.00) (Fig. S10†). The integrated areas of these chromatographic peaks confirm the presence of these isomers, in a ratio of 1 : 0.6. This result is consistent with the ones observed by NMR spectroscopy (Table S1†). The IR spectra of these complexes show peaks around 840 cm^{-1}, confirming the presence of the PF_6^- counter ion (Fig. S11 and S12†) in the obtained products. This observation is in agreement with the molar conductance of the complexes obtained in DMSO, which supported these compounds as hexafluorophosphate salts of the type 1 : 1 electrolytes.[47]

Although the isomers from **2a**/**2b** could not be isolated, suitable single crystals were obtained only for **2b** in a methanol/DCM (1 : 1) mixture for X-ray diffraction (XRD) experiments. Complex **2b** crystallizes in a monoclinic system, in a $P2_1/c$ space group. In this configuration, the ruthenium(II) ion lies on a distorted octahedral environment, coordinated to dppen moiety (P1 and P2), one bipy (N3 and N4), and a mercapto ligand in its deprotonated form (N1 and S1) (Fig. 2). In this structure, the S1 is coordinated *trans* to P1 while N1 is *trans* to N4. Furthermore, the Ru–S1 and Ru–N1 bond distances are 2.4602(4) and 2.0817(4) Å, respectively, which are in agreement with those observed for Ru(II)–mercapto-based complexes (for more information, see ESI, Table S2–S4†). For **1** and **2a**/**2b**, elemental analysis and ESI-HRMS results are in agreement with theoretical values (Fig. S13 and S14†). The UV-Vis

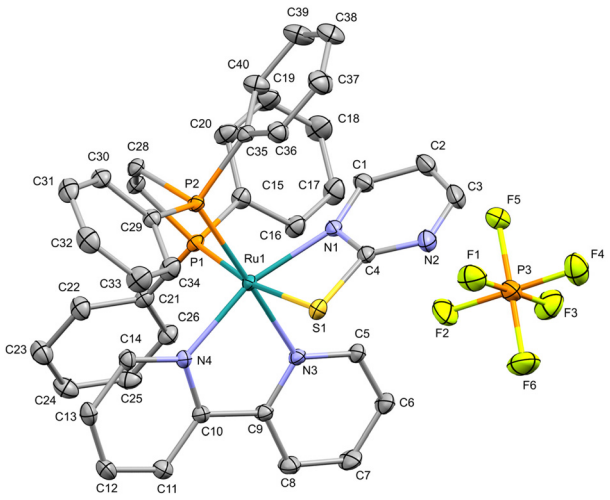

Fig. 2 The molecular structure of **2b** with displacement ellipsoids drawn at the 30% probability level. Hydrogen atoms are excluded for clarity.

spectra of the complexes recorded in DMSO (Fig. S15†) revealed the presence of a band with absorption at 298 nm, centered in the ancillary ligands. Additionally, a second one can be observed around 402 nm, which is characteristic of metal-to-ligand charge transfer (MLCT).[48]

The electrochemical behavior of the metal complexes was investigated by the cyclic voltammetry (CV) technique. Measurements in DCM revealed quasi-reversible processes, associated with the couple Ru(II)/Ru(III) (Table 1). As described

Table 1 Electrochemical behavior for Ru(II)–phosphine–mercapto complexes. Redox potentials are reported in V *versus* Ag/AgCl under N_2 in dry DCM. Scan rate: 50 mV s^{-1}

	E_{pa}	E_{pc}	$E_{1/2}$
[Ru(bipy)(dppen)(L1)] (**1**)	1.02	0.89	0.95
[Ru(bipy)(dppen)(L2)] (**2a**/**2b**)	1.16	1.06	1.11

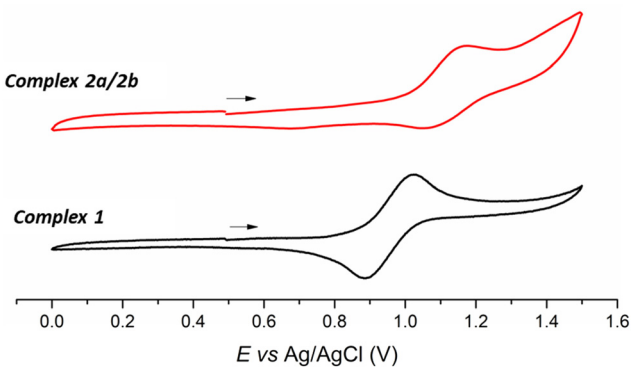

Fig. 3 Cyclic voltammogram of Ru(II)–phosphine–mercapto complexes **1** and **2a**/**2b** in DCM (0.1 mol L^{-1} TBAP). Scan rate 50 mV s^{-1}.

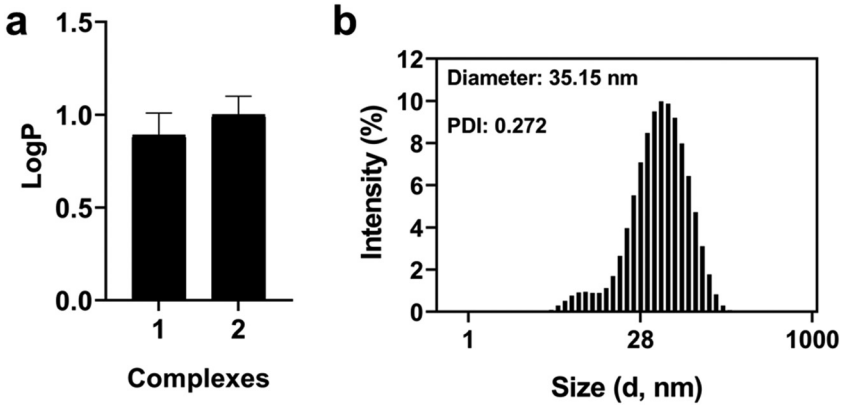

Fig. 4 Solubility and aggregation of Ru(II) complexes **1** and **2a**/**2b**. (a) Partition coefficient between *n*-octanol/PBS and (b) size distribution by the intensity (20 μM) in PBS 10% FBS.

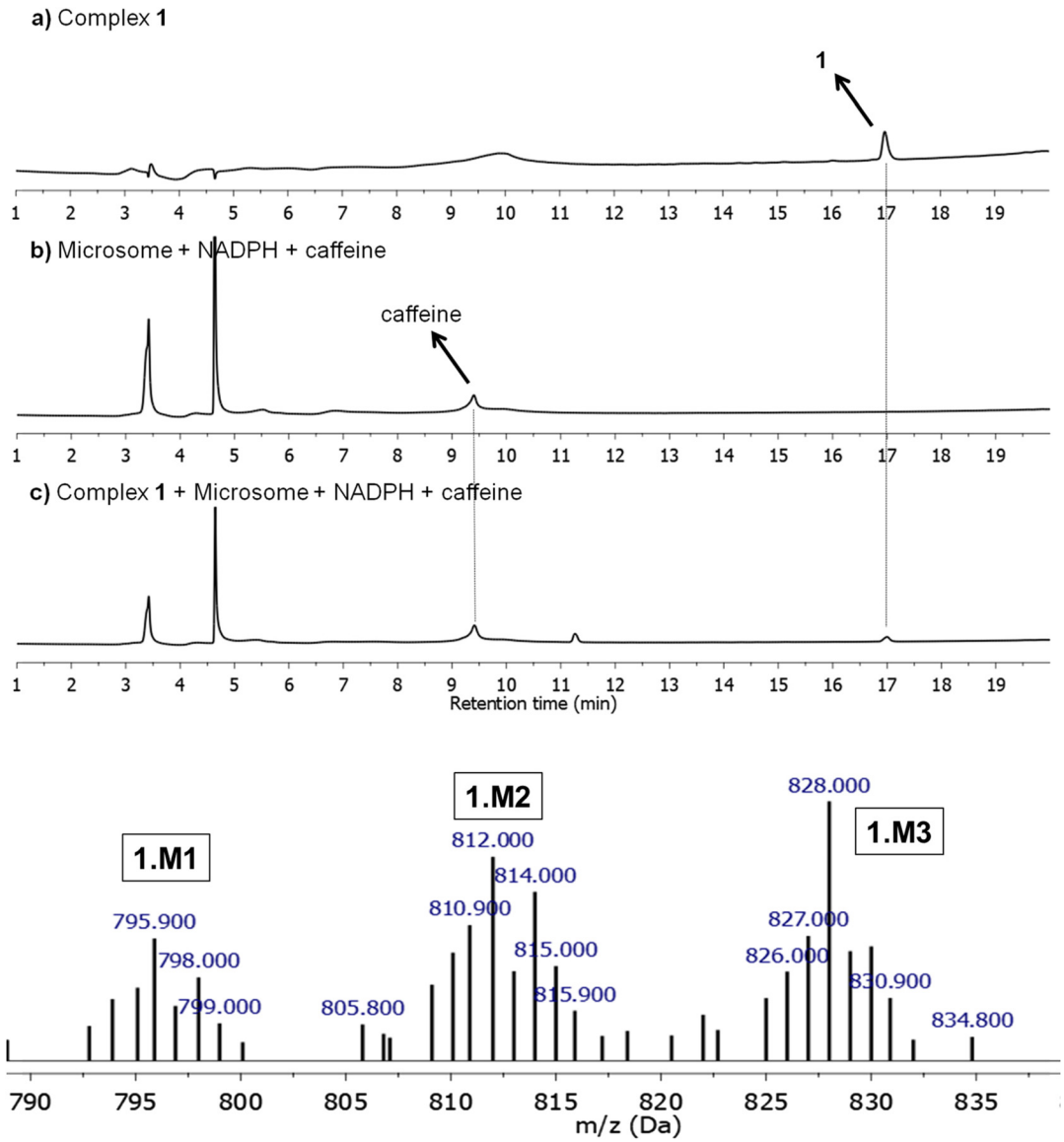

Fig. 5 Reversed-phase HPLC traces of **1** at 250 nm for 0 h and 48 h in cell culture medium/DMSO (DMEM supplemented with 10% fetal bovine serum, 2 mM L-glutamine and 100 U mL^{-1} of penicillin–streptomycin mixture).

in several metal-based systems, the metal-centered process can be modulated by the different donor/acceptor properties of the ligands.[49,50] In the present case, the chlorido replacement (π- and σ-donor) by the mercapto ligand (π-acceptor) changes the electron density over the Ru(II) center, providing a higher electrochemical stability.[37] Thus, the $E_{1/2}$ observed for the Ru(II)–phosphine complexes are found at 0.95 and 1.11 V *vs.* Ag/AgCl, respectively, which are the following values already reported for Ru(II)–phosphine–mercapto complexes (Fig. 3).[40,41]

The lipophilicity is an important parameter in drug design, playing a crucial role in the pharmacokinetic process. To assess this physicochemical property, the *n*-octanol/PBS partition coefficient (log *P*) of complexes **1** and **2a**/**2b** was determined by the shake-flask method.[51] These complexes were found principally in an organic layer. The results indicate a similar lipophilic profile for **1** (log *P* = 0.89 ± 0.12) and **2a**/**2b** (log *P* = 1.00 ± 0.10) with little deviations (Fig. 4). To investigate the possible aggregation of our ruthenium complexes in phosphate buffered saline (PBS), dynamic light scattering (DLS) experiments were performed in PBS containing 10% fetal bovine serum (FBS) (Fig. 4 and S16†). The low diameters and polydispersity indexes (PDIs) observed for both complexes suggests their stabilization due the presence of plasmatic proteins, as already reported in the literature.[52]

Stability studies

Since the stability of a drug in solution directly affects its biological profile, the stability of the compounds **1** and **2a**/**2b** was assessed. First, the $^{31}P\{^{1}H\}$ NMR spectra of the complexes were measured at different times in DMSO and DMSO containing 30% DMEM, over 48 h. No significant changes were detected in the samples, indicating their stability during this time (Fig. S17–S20†). The complexes were also found to be stable according to their UV-visible spectra recorded in DMSO solution over 48 h. Little changes were observed in their UV-Vis spectra in DMSO/PBS, indicating that most of these complexes remained stable during this time. Furthermore, their stabilities were also confirmed by HPLC in a cell culture medium containing 10% FBS, indicating their integrity in the biological environment over 48 h (Fig. S21–S25†).

Metabolic studies with human liver microsomes

Microsomal stability tests are crucial to evaluate the metabolic process of drug candidates and their ADME (absorption, distri-

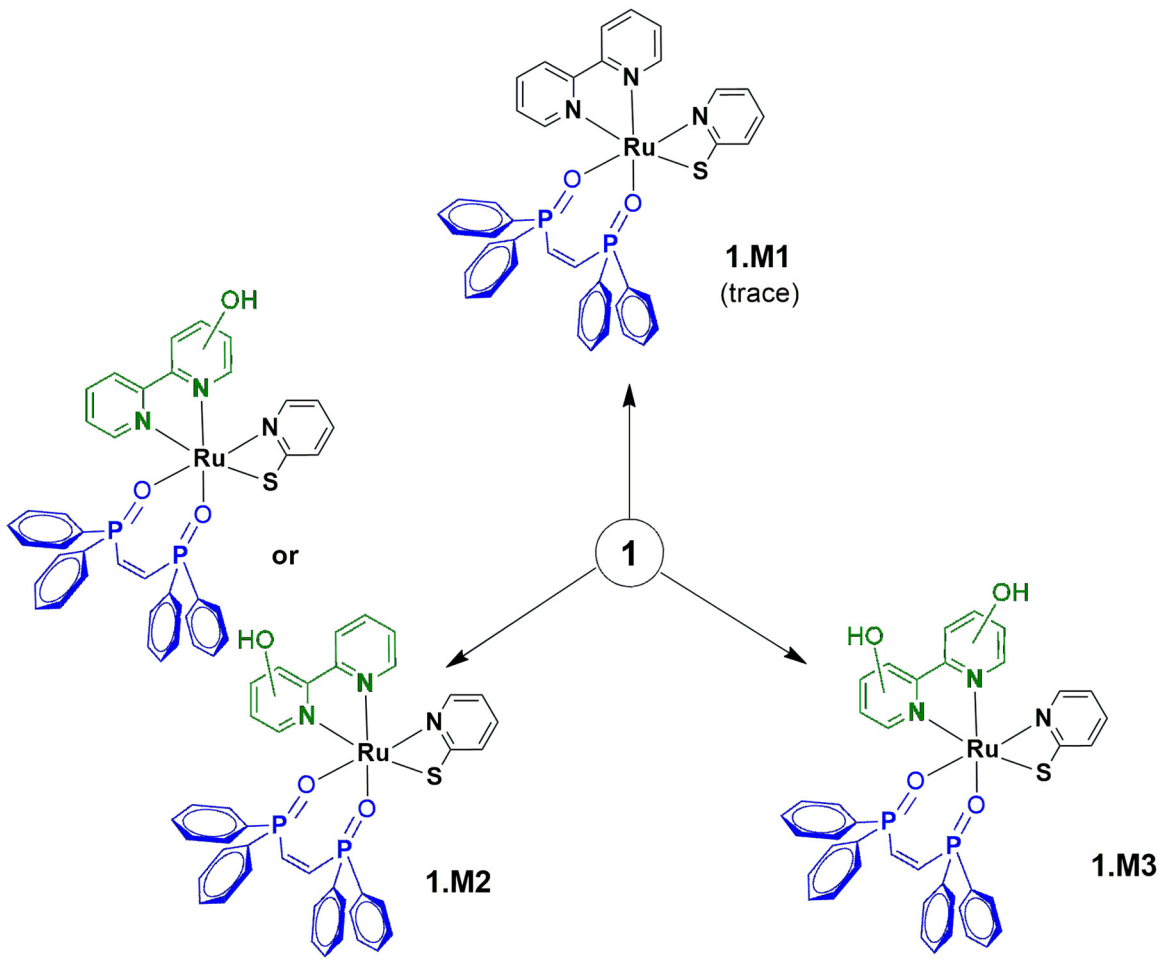

Scheme 2 Suggested metabolites identified for **1** after HLM incubation.

bution, metabolism & elimination) profile.[53] Since several drugs present a metabolism mediated *via* hepatic cytochrome P450 system, these approaches can be used to measure *in vitro* intrinsic clearance and identify possible metabolites eventually formed in solution.[54,55] Here, the metabolism of **1**, which was found to be the most promising compound of this study (see below), was investigated using human liver microsomes (HLM) that are fractions mostly derived from the endoplasmatic reticulum and are constituted by several enzymes from the cytochrome P450 system. Due to its inexpensive value and practical use, microsomes are employed to study *in vitro* drug metabolism, serving as screening to detect and characterize drug metabolites, playing an important role in the pharmacokinetic (PK) process. In this direction, **1** was incubated with HLM in the presence of NADPH (nicotinamide adenine dinucleotide phosphate), an enzyme co-factor of phase I metabolism, at 37 °C for 6 h. **1** only and microsomes in the presence of the co-factor were also prepared and caffeine was used as a standard control. As presented, **1** was detected at a retention time of 17.0 min, by LC-MS (positive ion electrospray mode) and remained unchanged with corresponding m/z^+ = 764.10 (Fig. 5 and S26†). In the presence of microsome/NADPH, a decrease of almost 14% of this peak in the LC spectrum was detected, indicating the consumption of the ruthenium(II) compound (Table S5†). It should be mentioned that peaks close to 3.4 and 4.7 min came from the microsome/NADPH mixture. The formation of metabolites **1.M1**, **1.M2**, and **1.M3** was confirmed upon ESI-MS analyses (Fig. 5 and S27†). These species were detected at a retention time of ~14.7 min in the HPLC experiment and present mass spectra patterns with peaks at m/z^+ = 795.90, 812.00, and 828.00, respectively (Fig. 5). The less abundant metabolite **1.M1** (<1%) has been obtained by oxidation of phosphorus in dppen ligand forming an O-coordinated pentavalent oxide (calculated m/z = 796.08). It should be mentioned that this coordination mode has already been reported for similar ruthenium-based compounds.[56,57] The most abundant metabolites **1.M2** and **1.M3** present peaks that match well the molecular weight of products formed from oxidation of bipy ligand (calculated m/z = 812.08 and 828.08) and can be associated with isomers containing hydroxyl group(s) at different positions on the aromatic ring. Similar results have been reported by Maximiano *et al.* which investigated Phase I and II

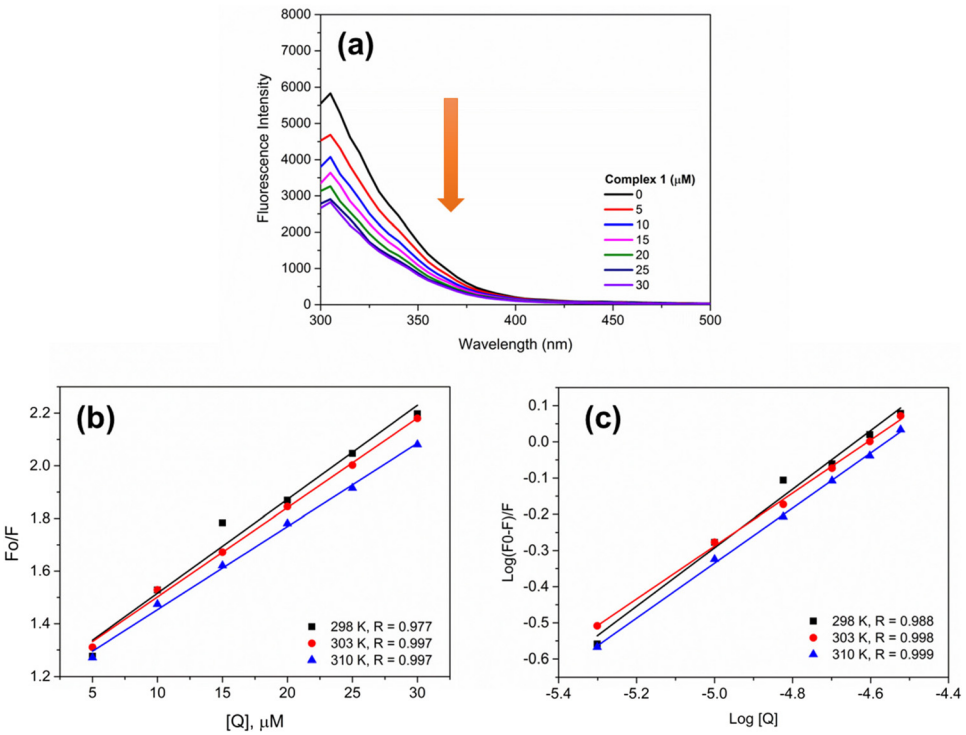

Fig. 6 (a) Fluorescence spectra of HSA (5 μM, λ_{ex} = 270 nm) in the absence and presence of **1** at different concentrations. (b) Stern–Volmer plot and (c) plot of log[($F_0 - F$)/F] *vs.* log[Q], at 298, 303 and 310 K.

Table 2 K_{SV}, k_q, K_b, n and ΔG parameters of the interaction of **1** with HSA

Complex	T (K)	K_{SV} (10^4, M^{-1})	k_q (10^{12}, M^{-1} s^{-1})	K_b (10^3, M^{-1})	n	ΔG (KJ mol^{-1})
1	298	3.77 ± 0.35	6.30	11.10 ± 0.11	0.87	−23.09 ± 5.29
	303	3.68 ± 0.40	6.10	6.37 ± 0.12	0.82	−22.08 ± 5.36
	310	3.44 ± 0.37	5.70	8.04 ± 0.12	0.85	−23.19 ± 5.47

Table 3 *In vitro* cytotoxicity (IC_{50}, μM) results against human breast cancer cells MDA-MB-231 and MCF-7, and non-cancerous breast cells MCF-10A cells after 48 h of incubation. Data are presented as mean ± SD of three independent replicates. **HL1**: 2-mercapto–pyridine; **HL2**: 2-mercapto–pyrimidine

	MDA-MB-231	MCF-7	MCF-10A	SI1	SI2
1	0.48 ± 0.04	1.64 ± 0.13	1.28 ± 0.08	2.7	0.78
2a/**2b**	0.35 ± 0.04	1.19 ± 0.09	0.79 ± 0.03	2.2	0.66
Precursor	>100	>100	>100	—	—
HL1	>100	>100	>100	—	—
HL2	>100	>100	>100	—	—
Cisplatin	12.43 ± 0.20	13.98 ± 0.40	23.90 ± 0.70	1.92	1.71

SI1 = IC_{50} MCF10A/IC_{50} MDA-MB-231; SI2 = IC_{50} MCF10A/IC_{50} MCF7.

metabolites from ruthenium-cyclopentadienyl anticancer compounds (Scheme 2).[58]

Human serum albumin interaction

Human serum albumin (HSA) is the most important transport protein present in the human circulatory system. The interaction between HSA and metal-based compounds is an important parameter that can affects the pharmacokinetic process. This interaction can occur *via* one or two binding sites of the protein, namely, site I (warfarin site) and site II (benzodiazepine site). Here, the interaction between **1** and HSA was

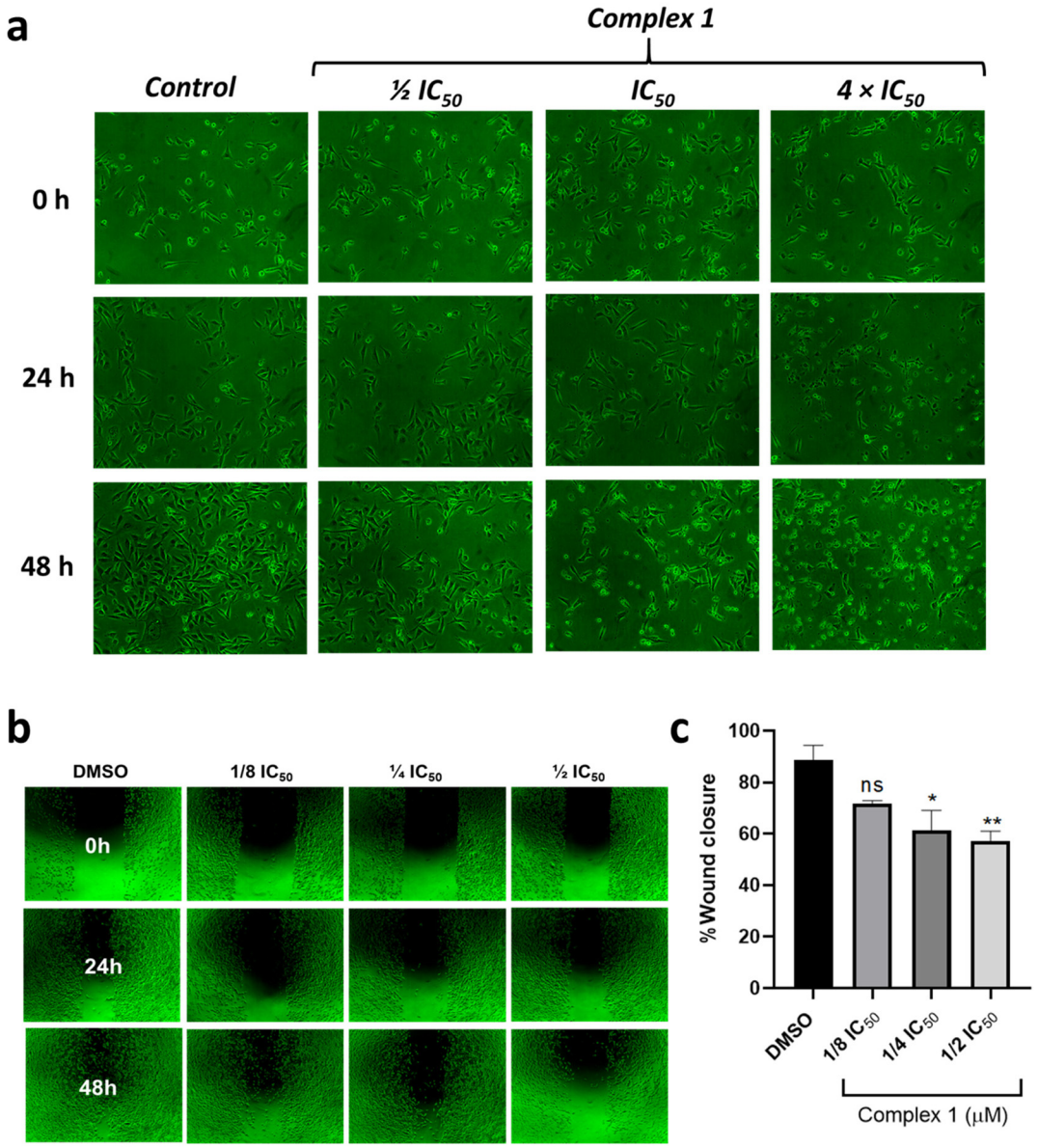

Fig. 7 (a) Microscopy images showing the cellular morphology of MDA-MB-231 cancer cells (10×) after 0, 24 and 48 h upon treatment with **1** at different concentrations. (b) Representative images of MDA-MB-231 cells after 48 h of treatment with **1**, were captured using an inverted microscope (4×). (c) Quantitative assessment of cell migration following treatment with **1**, conducted by measuring the extent of cell wound closure using Image J software. The statistical analysis was performed with a one-way ANOVA test followed by Dunnett's test (*p < 0.05; **p < 0.01). DMSO was employed as a negative control.

investigated *via* analysis of the fluorescence quenching of the protein in the presence of **1** (Fig. 6). To assess this effect, the Stern–Volmer relationship was applied. As observed in Table 2, the quenching constant (K_{SV}) was decreased with increasing temperature, indicating fluorescence suppression *via* a static mechanism. This implies the formation of a complex between the fluorophore and the suppressor in the ground state. Moreover, the bimolecular quenching rate constant (K_q) is in the order of 10^{12} M^{-1} s^{-1}, higher than the maximum for dynamic quenching ($k_q = 2.0 \times 10^{10}$ M^{-1} s^{-1}), also confirming this quenching mechanism.[36] The binding constant (K_b) was determined and the results indicate that **1** interacts with HSA with affinities in a similar order to other ruthenium(II) complexes.[59–61]

Furthermore, the K_{SV} and k_q parameters are similar to those obtained for the platinum drug oxaliplatin, implying that both compounds interact with serum albumin through a similar mechanism.[62]

The thermodynamic parameters free energy change ($\Delta G°$), entropy change ($\Delta S°$), and enthalpy ($\Delta H°$) were also obtained. The ΔG values indicate that the interaction occurs spontaneously at the temperature studied. In addition, negative values of ΔH and positive values for ΔS, as observed for **1**, −17.46 kJ mol^{-1} and 17.54 J mol^{-1}, respectively, indicate an interaction *via* electrostatic contacts.

Cytotoxicity studies

The cytotoxic profile of **1** and **2a**/**2b** was investigated in human breast cancer MDA-MB-231 [estrogen receptor-negative (ER−)] and MCF-7 [estrogen receptor-positive (ER+)] cells, as well as noncancerous breast MCF-10A cells after 48 h of incubation, using the colorimetric MTT assay. Complexes **1** and **2a**/**2b** are cytotoxic in all cell lines tested (Fig. S28 and S29†), and were found to be more cytotoxic in triple-negative breast cancer cells, with IC_{50} (μM) values lower than those obtained for cisplatin, 26- and 35-fold more potent, respectively. Although it shows high cytotoxicity on MDA-MB-231 cells (IC_{50} = 0.48 μM), unfortunately **1** also affects MCF-10A non-cancerous cells, exhibiting IC_{50} values of 1.28 μM. Despite this result, both metal complexes showed a higher selectivity index (SI) in MDA-MB-231 compared to the cisplatin control (Table 3). It should be mentioned that analogous Ru(II)–phosphine compounds were tested and their mixture of isomers presented similar IC_{50} values when compared to the isolated isomers.[45] The precursor and free ligands **HL1** and **HL2** are not cytotoxic at the maximum concentration tested. Thus, due to its promising results, **1** was selected for future biological studies.

Thus, the effect of **1** in the morphology of MDA-MB-231 cancer cells was investigated. After treatment of the cells during 48 h, a decrease in their density and adhesion was observed. Moreover, significant changes in the morphology of the cells were detected at higher concentrations, such as cell shrinkage and fragmentation, suggesting cell death/damage (Fig. 7).

Cell migration is an important process directly involved in tissue repair that can contribute to the formation of metastasis, playing a crucial role in cancer progression. Also, metastasis constitutes the main cause of death in cancer disease and remains poorly understood.[63,64] In this direction, the antimigratory capacity of **1** was investigated using the wound

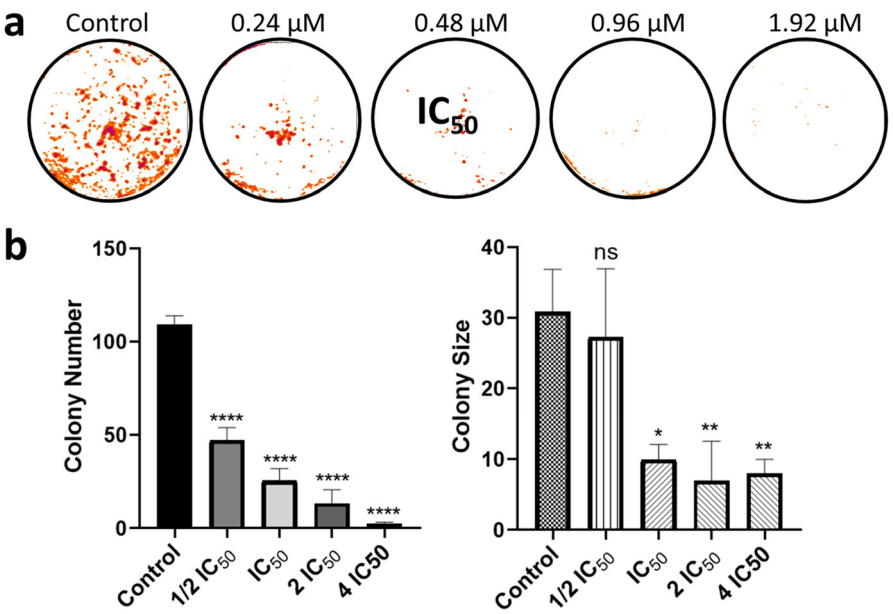

Fig. 8 Biological studies of **1** (a) assessment of the cell survival by clonogenic assay. Representative colony formation images of MDA-MB-231 cells after treatment with different concentrations of **1**. The study was performed in triplicate and the image represents one of them. (b) Quantitative data representing the colony number and size with relation to the concentration of **1**. Data are expressed as mean ± SD of three independent measurements. The statistical analysis was performed with one-way ANOVA test followed by Dunnett's test (*p < 0.05; **p < 0.01; ***p < 0.001 and ****p < 0.0001).

healing assay in MDA-MB-231 cells (Fig. 7). For this purpose, cells were seeded, and once they reached confluence, a scratch was made on the adherent cell monolayer using a sterile pipette tip. A culture medium containing **1** at different concentrations was added and the images were taken at 0, 24, and 48 h. Results presented in Fig. 8b reveal that, as expected, cells treated with DMSO had significant migratory potential. On the other hand, cells treated with **1** at concentrations of 0.06, 0.12, and 0.24 μM (1/8 IC_{50}, 1/4 IC_{50}, and 1/2 IC_{50} concentration) presented lower migration capacity and consequently lower percentage of wound closure, thus reflecting its potential as cell migration inhibitor.

Upon verifying the anti-migratory capacity, a clonogenic assay was performed to investigate how **1** affects colony formation in MDA-MB-231 cells (Fig. 8). The clonogenic assay measures the capacity of a single cell to form a colony of 50 or more cells *in vitro*.[65] Here, MDA-MB-231 cells were treated with different concentrations of **1**, and the colonies formed after 7 days were colored with violet-blue, washed, and dried. A decrease in the colony number upon treatment with **1** at 0.24 μM ($\frac{1}{2}$ IC_{50} concentration) was observed in Fig. 8. Also, the size of the colonies was drastically reduced in the presence of **1** at 0.48 μM (IC_{50} concentration) when compared to the untreated control, indicating the ability of **1** to reduce the clonogenic survival of MDA-MB-231 cells.

Conclusion

In this work [Ru(L1)(bipy)(dppen)]PF_6 (**HL1** = 2-mercapto–pyridine) (**1**) and [Ru(L2)(bipy)(dppen)]PF_6 (**HL2** = 2-mercapto–pyrimidine) (**2a**/**2b**) were synthesized and characterized. For **2b**, the crystal structure was solved by X-ray diffraction. The stability studies in different media revealed that **1** and both isomers **2a**/**2b** are stable under biological conditions. For **1**, microsomal stability with human liver microsomes/NADPH revealed three metabolites, containing oxidized dppen and/or bipy moieties. The Ru(II) complexes were found to be more cytotoxic than cisplatin, and **1** was 3-fold more selective against MDA-MB-231 cancer cells when compared to MCF-10A non-cancerous cells. Complex **1** was able to induce morphological alterations, inhibit the migration, and reduce the clonogenic survival in MDA-MB-231 cells, making it a promising cytotoxic agent against breast cancer.

Experimental section

Materials and instruments

All chemicals were of either reagent or analytical grade and were used as purchased from commercial sources without additional purification. $RuCl_3{\cdot}3H_2O$, 1,2-bis(diphenylphosphino)ethylene (dppen), 2-mercapto–pyridine (**HL1**) and 2-mercapto–pyrimidine (**HL2**) ligands were provided by Sigma Aldrich. All solvents were of analytical or HPLC grade. When necessary, solvents were degassed by purging with dry, oxygen-free nitrogen for at least 30 min before use. Microsomes were obtained from Gibco, NADPH tetrasodium salt from Sigma Aldrich, and caffeine from TCI Chemicals. ^1H, ^{31}P, and ^{13}C NMR spectra were recorded on a Bruker DRX 400 MHz spectrometer using CH_2Cl_2/D_2O or DMSO-d_6, and using the signal of the deuterated solvent as an internal standard. The chemical shifts (δ) are reported in ppm (parts per million) and coupling constants J are given in hertz (Hz). High-resolution ESI mass spectrometry (HR ESI-MS) experiments were carried out using a LTQ-Orbitrap XL from Thermo Scientific (Thermo Fisher Scientific, Courtaboeuf, France) and operated in positive ionization mode. Infrared spectra were recorded in a SpectrumTwo FTIR spectrometer (Perkin–Elmer) equipped with a Specac Golden GateTM ATR (attenuated total reflection) accessory; applied as neat samples; $1/\lambda$ in cm^{-1}. Elemental analyses were performed in the Microanalytical Laboratory at the Universidade Federal de São Carlos, São Carlos, Brazil, with an EA 1108 microanalyzer (Fisons Instruments) configured for % CHN. Analytical HPLC measurement was performed using the following system: 2xAgilent G1361 1260 Prep Pump system with an Agilent G7115 A 1260 DAD WR Detector equipped with an Agilent Pursuit XRs 5 C18 (100 Å, C18 5 μm 250 × 4.6 mm) Column and an Agilent G1364B 1260-FC fraction collector. The solvents (HPLC grade) were Millipore water (0.1% TFA, solvent A) and acetonitrile (0.1% TFA, solvent B). The HPLC gradients used are as follows: 0–1 min: isocratic 95% A (5% B); 1–12 min: linear gradient from 95% A (5% B) to 0% A (100% B); 12–14 min: isocratic 0% A (100% B); 14–15 min: linear gradient from 0% A (100% B) to 95% A (5% B). The flow rate was 1 mL min^{-1}. Detection was performed at 250 nm with a slit of 4 nm. The UV–Vis spectra were recorded on a Hewlett-Packard 8452A diode array or in a Varian Cary 8454" spectrophotometer using a 1 cm path length quartz cuvette. Conductivity values were obtained, at room temperature, using 1.0 mM solutions of the complexes in DCM in a Meter Lab CDM2300 instrument.

Synthesis of complexes

The metal complexes **1** and **2a**/**2b** were obtained from the *cis*-[$RuCl_2$(bipy)(dppen)] precursor. In a Schlenk flask containing 20 mL of methanol and 10 mL of DCM previously degassed, 11 mg (0.10 mmol) of respective mercapto ligand and 50 μL of Et_3N were added. After 30 min, 75 mg of precursor *cis*-[$RuCl_2$(bipy)(dppen)] (0.10 mmol) and 37 mg of KPF_6 were added. The mixture was refluxed for 24 h. After this period, the final volume was reduced to 3 mL approximately and water was added to induce the precipitation. The orange solid obtained was washed with water, diethyl ether, and dried under vacuum.

[Ru(L1)(bipy)(dppen)]PF_6 (**1**): yield (52 mg, 62%), $^{31}P\{^1H\}$ NMR (162 MHz, DMSO) δ 77.08 (d, J = 11.4 Hz), 74.16 (d, J = 11.5 Hz). ^1H NMR (400 MHz, DMSO) δ 9.64 (d, J = 3.2 Hz, 1H), 8.72 (t, J = 9.0 Hz, 1H), 8.58 (t, J = 9.1 Hz, 1H), 8.40 (dd, J = 16.7, 8.5 Hz, 2H), 8.26 (dd, J = 17.6, 8.6 Hz, 2H), 8.12 (t, J = 7.4 Hz, 1H), 7.79 (dd, J = 19.5, 8.3 Hz, 3H), 7.73–7.69 (m, 1H), 7.63 (d, J = 4.6 Hz, 1H), 7.56 (d, J = 7.1 Hz, 1H), 7.52–7.44 (m, 7H),

7.31 (s, 2H), 7.24 (t, J = 7.1 Hz, 1H), 7.16–7.10 (m, 2H), 7.08 (d, J = 7.1 Hz, 1H), 6.96–6.91 (m, 1H), 6.82 (t, J = 6.7 Hz, 2H), 6.70 (t, J = 7.3 Hz, 3H), 6.54 (d, J = 8.1 Hz, 1H), 6.29 (t, J = 8.6 Hz, 2H). ^{13}C NMR (101 MHz, DMSO) δ 181.40, 157.45, 155.85, 155.06, 151.62, 151.54, 151.62, 150.79, 150.60, 149.96, 149.38, 147.82, 138.95, 137.79, 136.24, 135.86, 134.29, 134.26, 134.14, 132.31, 132.06, 131.70, 130.60, 130.31, 129.25, 129.25, 127.84, 127.11, 126.03, 125.75, 124.68, 124.39, 124.06, 122.67, 117.75, 46.17. ESI-HRMS (positive detection mode): calculated for $C_{41}H_{34}N_3P_2RuS$ $[M]^+$ m/z 764.0987; Found 764.0969. Elemental analysis calculated for $C_{41}H_{34}F_6N_3P_3RuS{\cdot}0.2CH_3OH$ (%): C, 54.07; H, 3.83; N, 4.59; Found: C, 54.35; H, 4.22; N, 5.00. UV-Vis (DMSO): λ_{max} ($\varepsilon \times 10^{-3}$ M^{-1} cm^{-1}): 298 nm (32.46), 402 nm (5.48). IR: ν (cm^{-1}): 3672.34, 3053.73, 1966.26, 1601.75, 1544.88, 1579.52, 1482.80, 1434.90, 1469.48, 1420.72, 1444.11, 1275.91, 1311.04, 1244.33, 1158.66, 1138.27, 1097.62, 1071.04, 998.72, 840.85, 760.13, 698.36. The solvents (HPLC grade) were Millipore water (0.1% TFA, solvent A) and acetonitrile (0.1% TFA, solvent B). The HPLC gradients used are as follows: 0–1 min: isocratic 95% A (5% B); 1–12 min: linear gradient from 95% A (5% B) to 0% A (100% B); 12–14 min: isocratic 0% A (100% B); 14–15 min: linear gradient from 0% A (100% B) to 95% A (5% B). T_R = 12.471 min. Molar conductance (μS cm^{-1}, CH_2Cl_2): 42.19.

[Ru(L2)(bipy)(dppen)]PF_6 (**2a**/**2b**): yield (60 mg, 66%). ^{31}P $\{^1H\}$ NMR (162 MHz, DMSO) δ 79.70 (d, J = 6.0 Hz), 77.39 (d, J = 11.6 Hz), 74.97 (d, J = 11.6 Hz), 67.62 (d, J = 6.3 Hz). ^{1}H NMR (400 MHz, DMSO) δ 9.55 (s, 1H), 8.96–8.75 (m, 1H), 8.72 (t, J = 9.4 Hz, 1H), 8.59 (dd, J = 15.1, 8.2 Hz, 1H), 8.46 (t, J = 7.2 Hz, 2H), 8.36–8.12 (m, 6H), 7.94 (t, J = 2.9 Hz, 1H), 7.91–7.71 (m, 7H), 7.67 (d, J = 6.1 Hz, 2H), 7.64–7.47 (m, 12H), 7.26 (t, J = 7.1 Hz, 1H), 7.16 (t, J = 6.9 Hz, 2H), 7.12–7.04 (m, 2H), 7.03–6.94 (m, 2H), 6.90–6.77 (m, 6H), 6.69–6.62 (m, 2H), 6.49 (t, J = 8.8 Hz, 1H), 6.29 (t, J = 8.6 Hz, 2H), 6.04 (d, J = 3.3 Hz, 1H). ^{13}C NMR (101 MHz, DMSO) δ 156.11, 155.31, 133.68, 133.55, 132.39, 132.39, 131.41, 131.32, 130.14, 130.39, 129.28, 129.17, 127.79, 124.10, 40.57, 40.55, 39.78, 39.74, 39.53, 39.32. ESI-HRMS (positive detection mode): calculated for $C_{40}H_{33}N_4P_2RuS$ $[M]^+$ m/z 765.0939; found 765.0953. Elemental analysis calculated for $C_{40}H_{33}F_6N_4P_3RuS{\cdot}0.3H_2O$ (%): C, 52.50; H, 3.70; N, 6.12; found: C, 52.12; H, 3.36; N, 5.91. UV-Vis (DMSO): λ_{max} ($\varepsilon \times 10^{-3}$ M^{-1} cm^{-1}): 298 nm (17.07), 400 nm (2.91). IR: ν (cm^{-1}): 3667.03, 3054.27, 1966.77, 1602.18, 1562.57, 1540.24, 1469.93, 1482.65, 1434.72, 1375.10, 1311.40, 1249.45, 1187.90, 1161.39, 1070.67, 1097.21, 999.28, 841.72, 761.30, 698.60, 657.59. The solvents (HPLC grade) were Millipore water (0.1% TFA, solvent A) and acetonitrile (0.1% TFA, solvent B). The HPLC gradients used are as follows: 0–1 min: isocratic 95% A (5% B); 1–12 min: linear gradient from 95% A (5% B) to 0% A (100% B); 12–14 min: isocratic 0% A (100% B); 14–15 min: linear gradient from 0% A (100% B) to 95% A (5% B). T_R = 11.554 and 11.190 min. Molar conductance (μS cm^{-1}, CH_2Cl_2): 39.54.

X-ray crystallography

Single crystal X-ray diffraction data was collected at 160.0(1) K on a Rigaku OD Synergy/Hypix diffractometer using the copper X-ray radiation (λ = 1.54184 Å) from a dual wavelength X-ray source and an Oxford Instruments Cryojet XL cooler. The selected suitable single crystal was mounted using polybutene oil on a flexible loop fixed on a goniometer head and immediately transferred to the diffractometer. Pre-experiment, data collection, data reduction and analytical absorption correction[66] were performed with the program suite CrysAlisPro.[67] Using Olex2,[68] the structure was solved with the SHELXT[69] small molecule structure solution program and refined with the SHELXL2018/3 program package[70] by full-matrix least-squares minimization on F^2. PLATON[71] was used to check the result of the X-ray analysis. Supplementary crystallographic data for this paper have been deposited at the Cambridge Crystallographic Data Center, under the deposition numbers CCDC-2341519† (**2**).

Partition coefficient. Octanol/PBS partition coefficients (log Po/w) were determined using the shake-flask method. A total of 1 mg of each complex was solubilized in 1000 μL of DMSO and an aliquote of 50 μL was added to a mixture of equal volume of PBS (975 μL) and n-octanol (975 μL). The solutions were continuously shaken for 24 h at 1000 rpm and at 37 °C. Then, the samples were centrifuged for 5 min at 1000 rpm, and the organic and aqueous phases were separated. The organic phase was measured spectrophotometrically and the concentration was determined from a calibration curve (a linear regression) in order to obtain log P values = [complex(n-octanol)]/[complex(PBS)]. The experiments were carried out in triplicate.

DLS analysis. The size distributions by intensity and the PIs were determined by dynamic light scattering (DLS) using a Malvern ZetaSizer Nano ZS (scattering angle = 173°) at a temperature of 25 °C with an equilibrium time of 120 s. Stock solutions (2 mM) of the complexes in DMSO were filtered on a 0.22 μm membrane and were diluted at a concentration of 20 μM in filtered 10% FBS in PBS.

Human serum albumin (HSA) interaction. The interaction of **1** with HSA was investigated based on the suppression of HSA fluorescence in the presence of different concentrations of the complex at different temperatures. The protein interaction was examined in 96-well plates used for fluorescence assays. HSA (5.0 μM) was prepared by dissolving the protein in Tris-HCl at pH 7.4, and the complexes were dissolved in sterile DMSO. For the fluorescence measurements, the HSA concentration (950 μL) in the buffer Tris-HCl was kept constant in all samples, while the complex concentration (50 μL) was increased by 5.0, 10.0, 15.0, 20.0, 25.0 and 30.0 μM, and fluorescence emission spectra were obtained using a Synergy/H1-Biotek fluorometer with a monochromator, with excitation at 270 nm, and recorded in the 300 to 500 nm region. The experiments were carried out in triplicate and analyzed using the classical Stern–Volmer equation as follows:

$$F_0/F = 1 + k_q\tau_0[Q] = 1 + K_{SV}[Q] \quad (1)$$

where F_0 and F represent the fluorescence intensity in the absence and presence of the quencher (complex **1**), [Q]

denotes the concentration of the quencher, K_{SV} corresponds to the Stern–Volmer quenching constant, k_q stands for the biomolecular quenching constant, and τ_0 represents the average lifetime of HSA without the quencher ($\sim 10^{-8}$ s). The binding constant (K_b) and the number of binding sites (n) were determined using eqn (2), as follows:

$$\log[(F_0 - F)/F] = \log K_b + n \log[Q] \quad (2)$$

The thermodynamic parameters were derived from eqn (3) and (4):

$$\ln(K_{b2}/K_{b1}) = (1/T_1 - 1/T_2) \times \Delta H/R \quad (3)$$

$$\Delta G^\circ = -RT \ln K_b = \Delta H^\circ - T\Delta S^\circ \quad (4)$$

where K_1 and K_2 are the binding constants at temperatures T_1 and T_2, respectively, and R is the gas constant.

Microsomal stability assay. For each experiment, fresh stock solutions of complex **1** (10 mM) and caffeine (10 mM) were prepared in DMSO and H_2O, respectively. To 293 μL of PBS in an Eppendorf tube, 5 μL of microsomes (20 mg mL^{-1}) were added and the mixture was incubated for 5 min at 37 °C. Then, 5 μL of the complex and 20 μL of β-nicotinamide adenine dinucleotide phosphate (NADPH, 20 mM) were added and the resulting solutions were incubated for 6 h with continuous shaking at 600 rpm at 37 °C. After this period, the samples were quenched with 300 μL of methanol and 5 μL of caffeine was added. The final mixture was then shaken for additional 10 min. Subsequently, the samples were centrifuged for 10 min at 3000 rpm at 4 °C, filtered on a 0.22 μm membrane and analyzed by LCMS.[72] Controls containing only microsomes and complex **1** were also analyzed. The solvents (HPLC grade) were Millipore water (0.1% TFA, solvent A) and acetonitrile (0.1% TFA, solvent B). The HPLC gradients used are as follows: 0–3 min: isocratic 95% A (5% B); 3–18 min: isocratic 0% A (100% B); 18–20 min: isocratic 95% A (5% B).

Cell culture. The ruthenium complexes were tested against human breast cancer cells MDA-MB-231 (ATCC HTB-26) and MCF-7 (ATCC HTB-22) and non-cancer breast cells MCF-10A (ATCC CRL-10317). The cells were routinely maintained with Dulbecco's modified Eagle's medium DMEM high glucose (for MDA-MB-231), DMEM/F-12 (for MCF-10A) or Roswell Park Memorial Institute 1640 medium (RPMI 1640; for MCF-7), supplemented with 10% fetal bovine serum (FBS,), at 37 °C in a humidified 5% CO_2 atmosphere. MDA-MB-231 cell was adquried from Rio de Janeiro Cell Bank (BCRJ). MCF-7 and MCF-10A cells were kindly provided by Marcia R. Cominetti, UFSCar, São Carlos, SP, Brazil. Cell culture media were obtained from Vitrocell and FBS was obtained from Gibco.

Cytotoxicity. The cytotoxic of complexes **1** and **2a**/**2b** was investigated *via* 3-(4,5-dimethylthiazol-2-yl)-2,5-diphenyltetrazolium bromide (MTT) assay.[73] Cells were seeded in 150 μL of appropriate medium in 96-well plates and then incubated at 37 °C in 5% CO_2 for 24 h. The complexes were dissolved in DMSO, and 0.75 μL was added to wells (final concentration of 0.5% DMSO/well). Cells were incubated with the complexes for 48 h at 37 °C in 5% CO_2. Then, 50 μL of MTT (1 mg mL^{-1}) was added to each well. Cells were incubated again for 4 h, the medium was removed, and formazan crystals were solubilized in isopropyl alcohol. The absorbance was measured on a microplate spectrophotometer at 540 nm. All compounds were tested in three independent experiments performed in triplicate. DMSO was used as the negative control. The cell viability (IC_{50}) was determined using GraphPad Prism 8 software.

Morphological assay. The effect of complex **1** in the morphology of MDA-MB-231 breast cancer cells was investigated using 0.7×10^5 cells per well. The cells were seeded in a 12-well plate and after 24 h were exposed to different concentrations of ruthenium complex for an additional 48 h. Cells were examined at 0 and 48 h under an inverted optical microscope (NIKON ECLIPSE TS100) with a 10× objective lens, coupled with a Motcam 1SP camera. The morphological changes of the cells exposed to the treatment were compared to those treated with DMSO control.

Clonogenic survival assay. For the clonogenic assay, MDA-MB-231 breast cancer cells were used. A total of 500 cells were cultured per well in a 6-well plate. After 24 h, complex **1** was added in different concentrations. The plates were incubated at 37 °C in 5% CO_2 for 48 h. Then, the culture medium was replaced with a fresh medium and the plates were incubated for an additional 7 days. After this period, the culture medium was removed, and the colonies formed were fixed with a methanol solution of the violet crystal 0.5% for 30 min. Further, the plates were washed with water and dried at room temperature. The test was performed in triplicate. Relative survival was calculated using ImageJ software using the "Colony Area" Plug-in and the "Analyze Particles" function.

Cell migration assay. To evaluate the cell migration inhibition ability, we used the wound healing assay, where 1.0×10^5 cells per well were seeded in a 12-well plate maintained at 37 °C in a 5% CO_2 atmosphere for 24 h. After incubation, a wound was made using a sterile 1 mL pipette. The culture medium was changed, and different concentrations of complex **1** were added (0.01, 0.03 and 0.06 μM). Photos were recorded at times of 0, 24 and 48 h. The area of wound closure was calculated using Image J software.

Abbreviations

ADME	Absorption, distribution, metabolism & elimination
ATP	Adenosine triphosphate
CV	Cyclic voltammetry
DCM	Dichloromethane
DLS	Dynamic light scattering
DMEM	Dulbecco's modified Eagle's medium
FBS	Fetal bovine serum
HLM	Human liver microsomes
MTT	3-(4,5-Dimethylthiazol-2-yl)-2,5-diphenyltetrazolium bromide
NADPH	Nicotinamide adenine dinucleotide phosphate
PBS	Phosphate buffer saline
PDI	Polydispersity index

PK	Pharmacokinetic
RPMI	Roswell Park Memorial Institute 1640 medium
SI	Selectivity index
TBAP	Tetrabutylammonium phosphate

Data availability

Supplementary data to this article can be found online at https://doi.org/DOI.

Author contributions

Marcos V. Palmeira-Mello: investigation, methodology, validation, data curation and, writing – original draft. Analu R. Costa: investigation. Leticia P. de Oliveira: investigation. Olivier Blacque: investigation, resources and validation. Gilles Gasser: conceptualization, funding acquisition, supervision and writing – review & editing. Alzir A. Batista: conceptualization, funding acquisition, supervision and writing – review & editing.

Conflicts of interest

There are no conflicts to declare.

Acknowledgements

We thank FAPESP (process 2023/02475-8) and CNPq for financial support. M. V. P.-M. thanks the São Paulo State Research Support Foundation (FAPESP, processes 2021/01787-0 and 2022/09971-8). This work was financially supported by an ERC Consolidator Grant PhotoMedMet to G. G. (GA 681679) and has received support under the program "Investissements d'Avenir" launched by the French Government and implemented by the ANR with the reference ANR-10-IDEX-0001-02 PSL (G. G.).

References

1 D. Hanahan and R. A. Weinberg, *Cell*, 2000, **100**, 57–70, DOI: 10.1016/s0092-8674(00)81683-9.
2 D. Hanahan and R. A. Weinberg, *Cell*, 2011, **144**(4), 646–674, DOI: 10.1016/j.cell.2011.02.013.
3 *IARC, International Agency for Research on Cancer*, https://gco.iarc.fr/today/data/factsheets/cancers/20-Breast-fact-sheet.pdf, accessed on January, **2024**.
4 *WHO, World Health Organization*, https://www.who.int/news-room/fact-sheets/detail/breast-cancer, accessed on January, **2024**.
5 B. Rosenberg, L. VanCamp, J. Trosko and V. H. Mansour, *Nature*, 1969, **222**, 385–386, DOI: 10.1038/222385a0.
6 E. Ortega, C. Pérez-Arnaiz, V. Rodríguez, C. Janiak, N. Busto, B. García and J. Ruiz, *Eur. J. Med. Chem.*, 2021, **222**, 113600, DOI: 10.1016/j.ejmech.2021.113600.
7 V. Censi, A. B. Caballero, M. Pérez-Hernández, V. Soto-Cerrato, L. Korrodi-Gregório, R. Pérez-Tomás, M. M. Dell'Anna, P. Mastrorilli and P. Gamez, *J. Inorg. Biochem.*, 2019, **198**, 110749, DOI: 10.1016/j.jinorgbio.2019.110749.
8 S. Dasari and P. B. Tchounwou, *Eur. J. Pharmacol.*, 2014, **740**, 364–378, DOI: 10.1016/j.ejphar.2014.07.025.
9 J. Zhou, Y. Kang, L. Chen, H. Wang, J. Liu, S. Zeng and L. Yu, *Front. Pharmacol.*, 2020, **11**, 343, DOI: 10.3389/fphar.2020.00343.
10 R. Paprocka, M. Wiese-Szadkowska, S. Janciauskiene, T. Kosmalski, M. Kulik and A. Helmin-Basa, *Coord. Chem. Rev.*, 2022, **452**, 214307, DOI: 10.1016/j.ccr.2021.214307.
11 N. Muhammad and Z. Guo, *Curr. Opin. Chem. Biol.*, 2014, **19**, 144–153, DOI: 10.1016/j.cbpa.2014.02.003.
12 E. Ortega, G. Vigueras, F. J. Ballester and J. Ruiz, *Coord. Chem. Rev.*, 2021, **446**, 214129, DOI: 10.1016/j.ccr.2021.214129.
13 M. V. P. Mello, G. Cebrian-Torrejon, J. R. Pereira, C. S. Moreira, C. B. S. M. R. Gomes, D. R. Rocha, E. M. S. Fagundes, G. B. Ferreira and M. Lanznaster, *J. Inorg. Biochem.*, 2019, **199**, 110756, DOI: 10.1016/j.jinorgbio.2019.110756.
14 G. Golbaghi, I. Pitard, M. Lucas, M. M. Haghdoost, Y. L. de los Santos, N. Doucet, S. A. Patten, J. T. Sanderson and A. Castonguay, *Eur. J. Med. Chem.*, 2020, **188**, 112030, DOI: 10.1016/j.ejmech.2019.112030.
15 M. M. Haghdoost, J. Guard, G. Golbaghi and A. Castonguay, *Inorg. Chem.*, 2018, **57**, 7558–7567, DOI: 10.1021/acs.inorgchem.8b00346.
16 J. Kasparkova, A. Hernández-García, H. Kostrhunova, M. Goicuría, V. Novohradsky, D. Bautista, L. Markova, M. D. Santana, V. Brabec and J. Ruiz, *J. Med. Chem.*, 2024, **67**, 691–708, DOI: 10.1021/acs.jmedchem.3c01978.
17 A. Marco, P. Ashoo, S. Hernández-García, P. Martínez-Rodríguez, N. Cutillas, A. Vollrath, D. Jordan, C. Janiak, F. Gandía-Herrero and J. Ruiz, *J. Med. Chem.*, 2024, **67**, 7891–7910, DOI: 10.1021/acs.jmedchem.3c01869.
18 J. Grau, A. Caubet, O. Roubeau, D. Montpeyó, J. Lorenzo and P. Gamez, *ChemBioChem*, 2020, **17**, 2348–2355, DOI: 10.1002/cbic.202000154.
19 A. Notaro, M. Jakubaszek, N. Rotthowe, F. Maschietto, R. Vinck, P. S. Felder, B. Goud, M. Tharaud, I. Ciofini, F. Bedioui, R. F. Winter and G. Gasser, *J. Am. Chem. Soc.*, 2020, **142**, 6066–6084, DOI: 10.1021/jacs.9b12464.
20 S. Y. Lee, C. Y. Kim and T.-G. Nam, *Drug Des., Dev. Ther.*, 2020, **14**, 5375–5392, DOI: 10.2147/DDDT.S275007.
21 K. J. Franz and N. Metzler-Nolte, *Chem. Rev.*, 2019, **119**, 727–729, DOI: 10.1021/acs.chemrev.8b00685.
22 E. Boros, P. J. Dyson and G. Gasser, *Chem*, 2020, **6**, 41–60, DOI: 10.1016/j.chempr.2019.10.013.
23 G. Golbaghi and A. Castonguay, *Molecules*, 2020, **25**, 265, DOI: 10.3390/molecules25020265.

24 A. Notaro and G. Gasser, *Chem. Soc. Rev.*, 2017, **46**, 7317, DOI: 10.1039/c7cs00356k.
25 C. G. Hartinger, M. A. Jakupec, S. Zorbas-Seifried, M. Groessl, A. Egger, W. Berger, H. Zorbas, P. J. Dyson and B. K. Keppler, *Chem. Biodiversity*, 2008, **5**, 2140–2155, DOI: 10.1002/cbdv.200890195.
26 R. Trondl, P. Heffeter, C. R. Kowol, M. A. Jakupec, W. Berger and B. K. Keppler, *Chem. Sci.*, 2014, **5**, 2925–2932, DOI: 10.1039/C3SC53243G.
27 E. Alessio, G. Mestroni, A. Bergamo and G. Sava, *Curr. Top. Med. Chem.*, 2004, **4**, 1525–1535, DOI: 10.2174/1568026043387421.
28 F. J. Ballester, A. Hernández-García, M. D. Santana, D. Bautista, P. Ashoo, E. Ortega-Forte, G. Barone and J. Ruiz, *Inorg. Chem.*, 2024, **63**(14), 6202–6216, DOI: 10.1021/acs.inorgchem.3c04432.
29 F. J. Ballester, E. Ortega, D. Bautista, M. D. Santana and J. Ruiz, *Chem. Commun.*, 2020, **56**, 10301, DOI: 10.1039/d0cc02417a.
30 E. Ortega-Forte, A. Rovira, M. López-Corrales, A. Hernández-García, F. J. Ballester, E. Izquierdo-García, M. Jordà-Redondo, M. Bosch, S. Nonell, M. D. Santana, J. Ruiz, V. Marchán and G. Gasser, *Chem. Sci.*, 2023, **14**, 7170, DOI: 10.1039/d3sc01844j.
31 A.-C. Munteanu, A. Notaro, M. Jakubaszek, J. Cowell, M. Tharaud, B. Goud, V. Uivarosi and G. Gasser, *Inorg. Chem.*, 2020, **59**, 4424–4434, DOI: 10.1021/acs.inorgchem.9b03562.
32 S. J. Steinke, S. Gupta, E. J. Piechota, C. E. Moore, J. J. Kodanko and C. Turro, *Chem. Sci.*, 2022, **13**, 1933–1945, DOI: 10.1039/d1sc05647f.
33 A. P. Lanquist, S. Gupta, K. F. Al-Afyouni, M. Al-Afyouni, J. J. Kodanko and C. Turro, *Chem. Sci.*, 2021, **12**, 12056–12067, DOI: 10.1039/d1sc03213e.
34 R. J. Mitchell, A. S. Gowda, A. G. Olivelli, A. J. Huckaba, S. Parkin, J. M. Unrine, V. Oza, J. S. Blackburn, F. Ladipo, D. K. Heidary and E. C. Glazer, *Inorg. Chem.*, 2023, **62**, 10940–10954, DOI: 10.1021/acs.inorgchem.3c00736.
35 G. F. Grawe, K. M. Oliveira, C. M. Leite, T. D. de Oliveira, A. R. Costa, C. A. F. Moraes, J. Honorato, M. R. Cominetti, E. E. Castellano, R. S. Correa, S. P. Machado and A. A. Batista, *J. Inorg. Biochem.*, 2023, **244**, 112204, DOI: 10.1016/j.jinorgbio.2023.112204.
36 G. F. Grawe, K. M. Oliveira, C. M. Leite, T. D. de Oliveira, J. Honorato, A. G. Ferreira, E. Castellano, M. R. Cominetti, R. S. Correa and A. A. Batista, *Dalton Trans.*, 2022, **51**, 1489–1501, DOI: 10.1039/D1DT02851K.
37 A. Saha, I. Mondal, A. Kumari, A. K. Sonkar, R. Mishra, R. Kulshreshtha and A. K. Patra, *Dalton Trans.*, 2024, **53**, 1551–1567, DOI: 10.1039/D3DT02941G.
38 L. Rafols, D. Josa, D. Aguilà, L. A. Barrios, O. Roubeau, J. Cirera, V. Soto-Cerrato, R. Pérez-Tomás, M. Martínez, A. Grabulosa and P. Gamez, *Inorg. Chem.*, 2021, **60**, 7974–7990, DOI: 10.1021/acs.inorgchem.1c00507.
39 M. M. da Silva, M. S. de Camargo, S. Castelli, R. A. de Grandis, E. E. Castellano, V. M. Deflon, M. R. Cominetti, A. Desideri and A. A. Batista, *J. Braz. Chem. Soc.*, 2020, **31**(3), 536–549, DOI: 10.21577/0103-5053.20190214.
40 G. H. Ribeiro, A. P. M. Guedes, T. D. de Oliveira, C. R. S. T. B. de Correia, L. Colina-Vegas, M. A. Lima, J. A. Nóbrega, M. R. Cominetti, F. V. Rocha, A. G. Ferreira, E. E. Castellano, F. R. Teixeira and A. A. Batista, *Inorg. Chem.*, 2020, **59**, 15004–15018, DOI: 10.1021/acs.inorgchem.0c01835.
41 M. M. da Silva, G. H. Ribeiro, M. S. de Camargo, A. G. Ferreira, L. Ribeiro, M. I. F. Barbosa, V. M. Deflon, S. Castelli, A. Desideri, R. S. Corrêa, A. B. Ribeiro, H. D. Nicolella, S. D. Ozelin, D. C. Tavares and A. A. Batista, *Inorg. Chem.*, 2021, **60**, 14174–14189, DOI: 10.1021/acs.inorgchem.1c01539.
42 A. Notaro, A. Frei, R. Rubbiani, M. Jakubaszek, U. Basu, S. Koch, C. Mari, M. Dotou, O. Blacque, J. Gouyon, F. Bedioui, N. Rotthowe, R. F. Winter, B. Goud, S. Ferrari, M. Tharaud, M. Řezáčová, J. Humajová, P. Tomšík and G. Gasser, *J. Med. Chem.*, 2020, **63**, 5568–5584, DOI: 10.1021/acs.jmedchem.0c00431.
43 K. Słoczyńska, A. Gunia-Krzyżak, P. Koczurkiewicz, K. Wójcik-Pszczoła, D. Żelaszczyk, J. Popiół and E. Pękala, *Acta Pharm.*, 2019, **69**, 345–361, DOI: 10.2478/acph-2019-0024.
44 E. Ortega-Forte, S. Hernández-García, G. Vigueras, P. Henarejos-Escudero, N. Cutillas, J. Ruiz and F. Gandía-Herrero, *Cell. Mol. Life Sci.*, 2022, **79**, 510, DOI: 10.1007/s00018-022-04526-5.
45 K. M. Oliveira, E. J. Peterson, M. C. Carroccia, M. R. Cominetti, V. M. Deflon, N. P. Farrell, A. A. Batista and R. S. Correa, *Dalton Trans.*, 2020, **49**, 16193, DOI: 10.1039/d0dt01091j.
46 M. M. da Silva, M. S. de Camargo, R. S. Correa, S. Castelli, R. A. De Grandis, J. E. Takarada, E. A. Varanda, E. E. Castellano, V. M. Deflon, M. R. Cominetti, A. Desideri and A. A. Batista, *Dalton Trans.*, 2019, **48**, 14885, DOI: 10.1039/c9dt01905g.
47 W. J. Geary, *Coord. Chem. Rev.*, 1971, **7**, 81–122, DOI: 10.1016/S0010-8545(00)80009-0.
48 V. D. S. Velozo-Sá, L. R. Pereira, A. P. D. Lima, F. Mello-Andrade, M. D. R. M. Rezende, R. M. Goveia, W. C. Pires, M. M. Silva, K. Oliveira, A. G. Ferreira, J. A. Ellena, V. M. Deflon, C. Grisolia, A. A. Batista and E. D. P. Silveira-Lacerda, *Dalton Trans.*, 2019, **48**, 6026–6039, DOI: 10.1039/C8DT03738H.
49 M. V. Palmeira-Mello, A. B. Caballero, J. M. Ribeiro, E. M. Souza-Fagundes, P. Gamez and M. Lanznaster, *J. Inorg. Biochem.*, 2020, **211**, 111211, DOI: 10.1016/j.jinorgbio.2020.111211.
50 P. Zhang and P. J. Sadler, *Eur. J. Inorg. Chem.*, 2017, **12**, 1541–1548, DOI: 10.1002/ejic.201600908.
51 E. Baka, J. E. A. Comer and K. Takács-Novák, *J. Pharm. Biomed. Anal.*, 2008, **46**, 335–341, DOI: 10.1016/j.jpba.2007.10.030.
52 R. Vinck, A. Gandioso, P. Burckel, B. Saubamea, K. Cariou and G. Gasser, *Inorg. Chem.*, 2022, **61**, 13576–13585, DOI: 10.1021/acs.inorgchem.2c02214.

53 K. M. Knights, D. M. Stresser, J. O. Miners and C. L. Crespi, *Curr. Protoc. Pharmacol.*, 2016, **74**, 781, DOI: 10.1002/cpph.9.
54 M. Patra, K. Ingram, A. Leonidova, V. Pierroz, S. Ferrari, M. N. Robertson, M. H. Todd, J. Keiser and G. Gasser, *J. Med. Chem.*, 2013, **56**(22), 9192–9198, DOI: 10.1021/jm401287m.
55 A. Zamora, C. A. Denning, D. K. Heidary, E. Wachter, L. A. Nease, J. Ruiz and E. C. Glazer, *Dalton Trans.*, 2017, **46**, 2165, DOI: 10.1039/c6dt04405k.
56 M. P. Felicissimo, A. A. Batista, A. G. Ferreira, J. Ellena and E. E. Castellano, *Polyhedron*, 2005, **24**, 1063–1070, DOI: 10.1016/j.poly.2005.02.026.
57 A. Gallen, A. Riera, X. Verdaguer and A. Grabulosa, *Catal. Sci. Technol.*, 2019, **9**, 5504, DOI: 10.1039/c9cy01501a.
58 I. Maximiano, C. Henriques, R. G. Teixeira, F. Marques, A. Valente and A. M. M. Antunes, *J. Inorg. Biochem.*, 2024, **251**, 112436, DOI: 10.1016/j.jinorgbio.2023.112436.
59 J. Shi, L. Xie, W. Gong, H. Bai, W. Wang, A. Wang, W. Cao, H. Tong and H. Wang, *Metallomics*, 2024, **16**, mfae005, DOI: 10.1093/mtomcs/mfae005.
60 R. S. Correa, L. M. Bomfim, K. M. Oliveira, D. R. M. Moreira, M. B. P. Soares, J. Ellena, D. P. Bezerra and A. A. Batista, *J. Inorg. Biochem.*, 2019, **198**, 110751, DOI: 10.1016/j.jinorgbio.2019.110751.
61 K. M. Oliveira, J. Honorato, G. R. Gonçalves, M. R. Cominetti, A. A. Batista and R. S. Correa, *Dalton Trans.*, 2020, **49**(36), 1264312652, DOI: 10.1039/D0DT01591A.
62 T. Lemma and J. Pawliszyn, *J. Pharm. Biomed. Anal.*, 2009, **50**, 570–575, DOI: 10.1016/j.jpba.2008.10.028.
63 S. A. Eccles and D. R. Welch, *Lancet*, 2007, **369**, 1742–1757, DOI: 10.1016/S0140-6736(07)60781-8.
64 J. Fares, M. Y. Fares, H. H. Khachfe, H. A. Salhab and Y. Fares, *Signal Transduction Targeted Ther.*, 2020, **5**, 28, DOI: 10.1038/s41392-020-0134-x.
65 N. A. P. Franken, H. M. Rodermond, J. Stap, J. Haveman and C. van Bree, *Nat. Protoc.*, 2006, **1**, 2315–2319, DOI: 10.1038/nprot.2006.339.
66 R. C. Clark and J. S. Reid, *Acta Crystallogr., Sect. A: Found. Crystallogr.*, 1995, **51**, 887, DOI: 10.1107/S0108767395007367.
67 *CrysAlisPro (version 1.171.42.75a)*, Rigaku Oxford Diffraction Ltd, Yarnton, Oxfordshire, England, 2022.
68 O. V. Dolomanov, L. J. Bourhis, R. J. Gildea, J. A. K. Howard and H. Puschmann, *J. Appl. Crystallogr.*, 2009, **42**, 339, DOI: 10.1107/S0021889808042726.
69 G. M. Sheldrick, *Acta Crystallogr., Sect. A: Found. Adv.*, 2015, **71**, 3–8, DOI: 10.1107/S2053273314026370.
70 G. M. Sheldrick, *Acta Crystallogr., Sect. C: Struct. Chem.*, 2015, **71**, 3–8, DOI: 10.1107/S2053229614024218.
71 A. L. Spek, *Acta Crystallogr., Sect. D: Biol. Crystallogr.*, 2009, **65**, 148, DOI: 10.1107/S090744490804362X.
72 S. Keller, Y. C. Ong, Y. Lin, K. Cariou and G. Gasser, *J. Organomet. Chem.*, 2020, **906**, 121059, DOI: 10.1016/j.jorganchem.2019.121059.
73 T. Mosmann, *J. Immunol. Methods*, 1983, **65**, 55–63, DOI: 10.1016/0022-1759(83)90303-4.